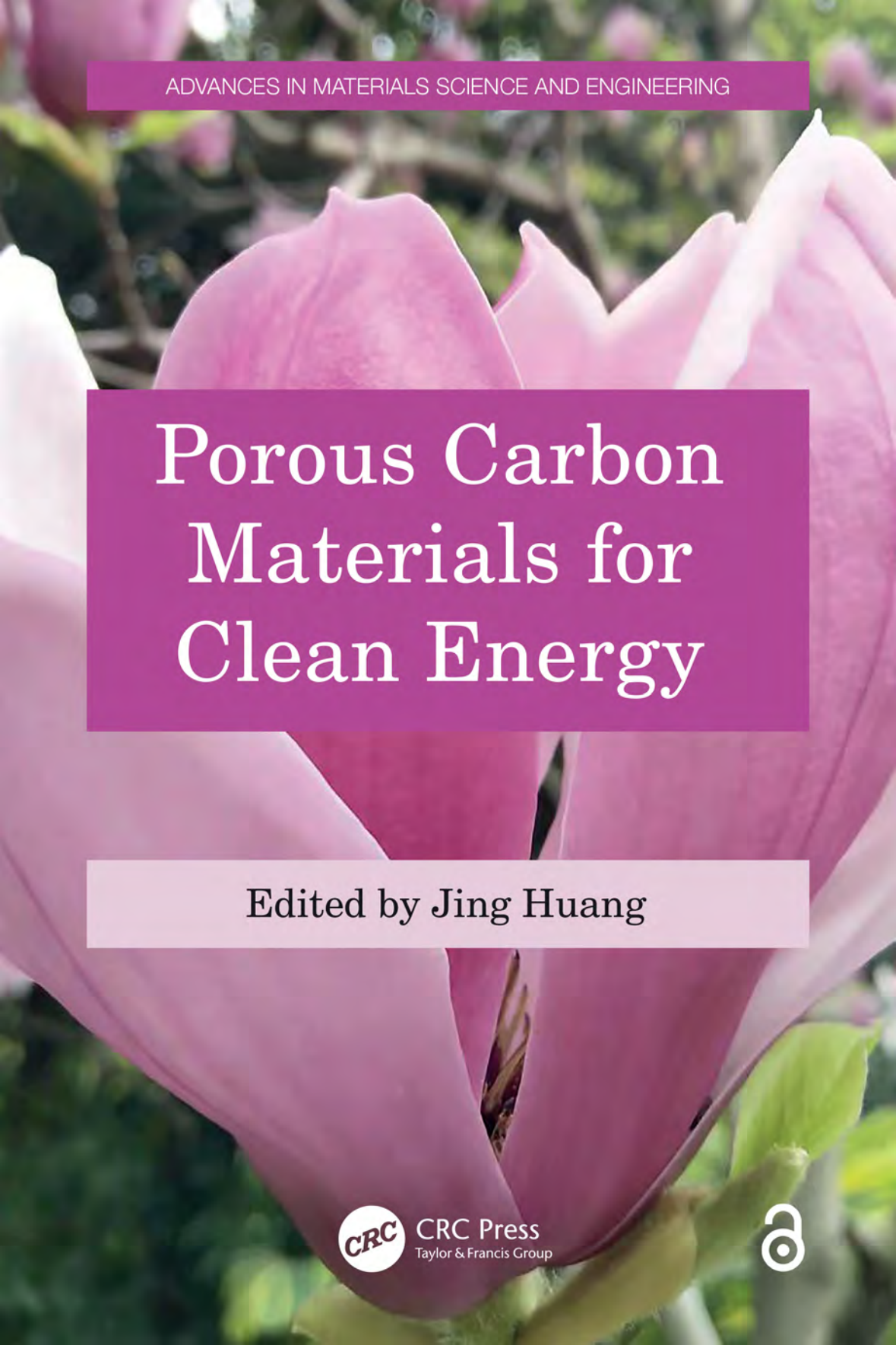
ADVANCES IN MATERIALS SCIENCE AND ENGINEERING
Porous Carbon Materials for Clean Energy
Edited by Jing Huang
CRC
CRC Press
Taylor & Francis Group

Porous Carbon Materials for Clean Energy

Porous carbons are widely used as electrode materials for supercapacitors owing to their high specific surface areas, abundant surface functionalities, well-controlled pore systems, and excellent conductivity and stability. New carbon materials with well-defined nanostructures and functionalization patterns have been developed to meet challenges of a growing global demand for energy-saving materials and sustainable materials to reduce negative environmental consequences. This book describes progress toward the conversion and efficient utilization of porous carbon and its derived precursor as electrode materials for clean energy.

- Explores the chemical structure, composition, properties, classification, and application of various porous carbon nanoparticles and nanostructured materials for clean energy uses.
- Proposes strategies for porous carbon production through featured examples.
- Covers a variety of materials, including those derived from biomass, graphene, aerogels, and carbon nanofibers.
- Discusses applications including electrocatalysts, batteries, hydrogen production, supercapacitors, and energy storage.
- Examines challenges and future opportunities.

This book will be of interest to materials and chemical engineers, scientists, researchers, and others active in advancing the development of renewable and clean energy technologies.

Jing Huang received his M.S. and Ph.D. degrees in organic chemistry in 2009 and 2012 from Southwest University, China, and served as a postdoctoral research fellow under the supervision of Prof. Chang Ming Li. He teaches at the College of Sericulture, Textile, and Biomass Sciences, Southwest University, China, and his research interests focus on nanomaterials derived from biomass for electrochemical applications such as energy storage and conversion.

Porous Carbon Materials for Clean Energy

Edited by Jing Huang

CRC Press
Taylor & Francis Group
Boca Raton London New York

CRC Press is an imprint of the
Taylor & Francis Group, an **informa** business

Designed cover image: © Jing Huang

First edition published 2025
by CRC Press
2385 NW Executive Center Drive, Suite 320, Boca Raton FL 33431

and by CRC Press
4 Park Square, Milton Park, Abingdon, Oxon, OX14 4RN

CRC Press is an imprint of Taylor & Francis Group, LLC

ISBN: 978-1-032-48173-9 (hbk)
ISBN: 978-1-032-48189-0 (pbk)
ISBN: 978-1-003-38783-1 (ebk)

DOI: 10.1201/9781003387831

Typeset in Times LT Std
by codeMantra

The electronic version of this book was funded to publish Open Access through Taylor & Francis' Pledge to Open, a collaborative funding open access books initiative. The full list of pledging institutions can be found on the Taylor & Francis Pledge to Open webpage.

Contents

Contributors

Paul K. Chu
Department of Physics
Department of Materials Science and Engineering, and Department of Biomedical Engineering
City University of Hong Kong
Kowloon, Hong Kong, P.R. China

Biao Gao
The State Key Laboratory of Refractories and Metallurgy
Institute of Advanced Materials and Nanotechnology
Wuhan University of Science and Technology
Wuhan, Hubei, P.R. China

Cheng Huang
School of New Energy and Materials
Southwest Petroleum University
Chengdu, P.R. China

Jing Huang
State Key Laboratory of Resource Insects
Key Laboratory of Sericultural Biology and Genetic Breeding
Ministry of Agriculture and Rural Affairs
College of Sericulture, Textile and Biomass Sciences
Southwest University
Chongqing, P.R. China

Tieqi Huang
College of Chemistry and Chemical Engineering
Central South University
Changsha, Hunan, P.R. China

Yongfa Huang
School of Light Industry and Engineering
State Key Laboratory of Pulp and Paper Engineering
South China University of Technology
Guangzhou, Guangdong, P.R. China

Kaifu Huo
Wuhan National Laboratory for Optoelectronics
Huazhong University of Science and Technology
Wuhan, Hubei, P.R. China

Gaojie Li
The State Key Laboratory of Refractories and Metallurgy
Institute of Advanced Materials and Nanotechnology
Wuhan University of Science and Technology
Wuhan, Hubei, P.R. China

Ruchun Li
Faculty of Chemistry and Chemical Engineering
Yunnan Normal University
Kunming, Yunnan, P.R. China

Ting Li
College of Chemistry
Xiangtan University
Xiangtan, Hunan Province, P.R. China

Yueming Li
State Key Laboratory of Metastable Materials Science and Technology
College of Materials Science and Engineering
Yanshan University
Qinhuangdao, P.R. China

Bei Liu
College of Chemistry
Xiangtan University
Xiangtan, Hunan Province, P.R. China

Wenxing Miao
Key Laboratory of Eco-functional Polymer Materials of the Ministry of Education
Key Laboratory of Polymer Materials of Gansu Province
College of Chemistry and Chemical Engineering
Northwest Normal University
Lanzhou, Gansu, P.R. China

Hui Peng
Key Laboratory of Eco-functional Polymer Materials of the Ministry of Education
Key Laboratory of Polymer Materials of Gansu Province
College of Chemistry and Chemical Engineering
Northwest Normal University
Lanzhou, Gansu, P.R. China

Xinwen Peng
School of Light Industry and Engineering
State Key Laboratory of Pulp and Paper Engineering
South China University of Technology
Guangzhou, Guangdong, P.R. China

Yan Song
Key Laboratory of Carbon Materials
Institute of Coal Chemistry
Chinese Academy of Sciences
Taiyuan, Shanxi, P.R. China

Xiaodong Tian
Key Laboratory of Carbon Materials
Institute of Coal Chemistry
Chinese Academy of Sciences
Taiyuan, Shanxi, P.R. China

Gang Wang
College of Materials and Engineering
Sichuan University
Chengdu, Sichuan Province, P.R. China

Jiale Xie
School of New Energy and Materials
Southwest Petroleum University
Chengdu, P.R. China

Pingping Yang
School of New Energy and Materials
Southwest Petroleum University
Chengdu, P.R. China

Tao Yang
Key Laboratory of Carbon Materials
Institute of Coal Chemistry
Chinese Academy of Sciences
Taiyuan, Shanxi, P.R. China

Yong Ye
College of Chemistry
Xiangtan University
Xiangtan, Hunan Province, P.R. China

Dingsheng Yuan
Department of Chemistry and Institute of Nanochemistry
Jinan University
Guangzhou, P.R. China

Linxin Zhong
School of Light Industry and Engineering
State Key Laboratory of Pulp and Paper Engineering
South China University of Technology
Guangzhou, Guangdong, P.R. China

Long Zou
College of Life Sciences
Jiangxi Normal University
Nanchang, Jiangxi, P.R. China

5 Biomass-Derived Graphene-Like Carbon Materials for Supercapacitor Applications

Gaojie Li, Biao Gao, Paul K. Chu and Kaifu Huo

1 INTRODUCTION

Fossil fuels are causing environmental problems and also getting depleted. Therefore, researchers have proposed renewable energy sources such as solar, wind, tide, and waste heat, which can provide energy without CO_2 emissions and pollutants. However, since renewable energy sources are often difficult to use on a large scale due to their geographical, intermittent, and unstable characteristics, the development of efficient energy conversion and storage technologies is highly required. The common electrochemical energy storage devices are rechargeable batteries and supercapacitors (SCs). SCs have attracted a lot of attention due to desirable characteristics such as the higher power density (1–103 kW kg^{-1}), faster charging/discharging capability, and longer cycling life (>106 cycles) compared to conventional lead-acid batteries and lithium-ion batteries.[1] In addition, SCs can be used in a wide temperature range (–70 to 85°C), whereas the use of conventional batteries is limited to a narrow temperature range. Owing to these excellent properties, SCs have great potential and value in future energy systems. Figure 5.1 depicts the Ragone plots of various energy storage systems.[2] Batteries can provide high energy densities of 150–500 Wh kg^{-1}, but their power density is limited due to the sluggish movement of electrons and ions. In order to maintain a high energy output, they are usually discharged for more than 10 min or even longer. In contrast, SCs with higher power densities can fully discharge in 10 s with an output power between 10 and 20 kW kg^{-1}. However, it is difficult for SCs to achieve energy densities of 30 Wh kg^{-1} or higher. As the key component in SCs, electrode materials have a decisive influence on the energy/power densities of SCs and therefore, the development of high-performance electrode materials is the hotspot for the SCs.

Carbonaceous materials are very important to electrochemical energy storage on account of their outstanding chemical stability, tunable porosity, large specific surface area (SSA), and abundant electroactive surface sites. Several carbon isomers

DOI: 10.1201/9781003387831-5

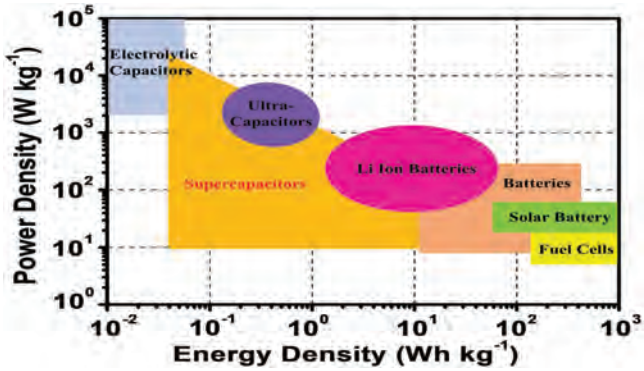

FIGURE 5.1 Ragone plots of various energy storage systems[2] (reproduced with permission: Copyright 2022, Royal Society of Chemistry).

have been utilized in electrodes and in particular, graphene has recently attracted great interest due to its distinct properties in terms of the electron conductivity (200 S m^{-1}), large SSA (2,630 $m^2 g^{-1}$), and high intrinsic carrier mobility (10,000 $cm^2 V^{-1} s^{-1}$).[3] With sp^2-hybridized carbon atoms arranged in a honeycomb-like network in a single plane, graphene is an ultrathin substance with high conductivity.[4] In addition, graphene with the long-range π–π conjugation possesses many attractive properties including chemical stability, thermal conductivity, and mechanical strength. However, there are some limitations for SCs application. First, large-scale synthesis is difficult and costly, and second, graphene layers undergo irreversible sheet stacking during electrode preparation, consequently reducing the active surface area and capacitance. Biomass-derived graphene-like carbon (BDGC) materials are excellent for SCs due to many virtues such as sustainability, reproducibility, abundant natural sources, and low cost.

In this chapter, recent progress in the preparation and capacitive properties of BDGC from biomass precursors are summarized and the common synthetic methods are described. The impact of the morphology, SSA, porous structure, and degree of graphitization on the electrochemical properties are discussed and future research directions are proposed.

1.1 Fundamentals of Supercapacitors

SCs also known as electrochemical capacitors or ultracapacitors have attracted considerable attention for electrochemical energy storage by bridging the gap between conventional dielectric capacitors and lithium-ion batteries. According to the charge storage mechanism, SCs are divided into three types: (1) Electric double-layer capacitors (EDLCs), which electrostatically store charges by adsorbing ions on the electrode surface; (2) Pseudocapacitors which electrochemically store energy *via* the rapid surface-controlled redox reactions with the Faraday types; (3) Hybrid capacitors which combine the electrodes with capacitive properties and battery-like performances to produce higher energy and power densities.

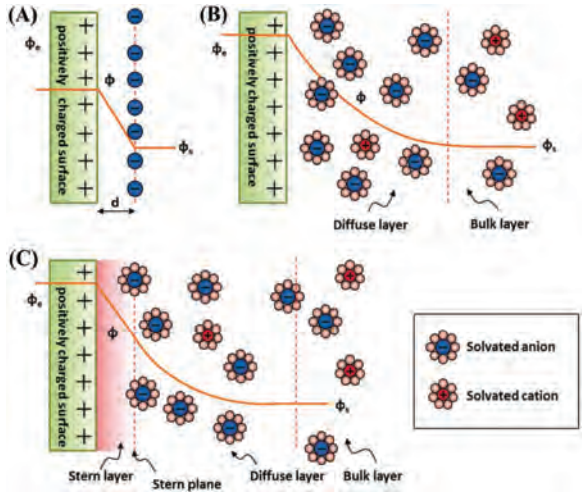

FIGURE 5.2 EDLC models: (A) Helmholtz, (B) Gouy–Chapman, and (C) Stern (reproduced with permission: Copyright 2014, Wiley-Blackwell).[5]

1.2 Charge Storage Mechanism

EDLCs store charge at the interface between the electrode and electrolyte via electrostatic ion adsorption/desorption. By applying a voltage between the electrodes, charges accumulate on the surface of the electrode, which is balanced by the adsorption of oppositely charged ions from the electrolyte. To avert short circuits, the two electrodes of EDLCs are separated by a separator. At the interface between the electrode and electrolyte, two layers of reverse charges are established during charging. EDLCs are comparable to parallel plate capacitors when an electrode of surface area S (m^2) is polarized, as shown in Figure 5.2.[5] Originally, the storage mechanism of EDLCs follows the Helmholtz model which describes the charge distribution at the interface (Figure 5.2A). The double layers (DL) of opposite charges are formed at the interface with an effective thickness (d) equal to the atomic distance. The potential in the vicinity of the electrode is gradually lowered and the simplified Helmholtz double layer can be envisioned as an electrical capacitor with a capacitance of C_H defined by Eqn 5.1:

$$C_H = \frac{\varepsilon_r \varepsilon_0 S}{d} \tag{5.1}$$

where ε_r is the dielectric constant of the electrolyte, ε_0 is the relative dielectric constant of vacuum ($\varepsilon_0 = 8.854 \times 10^{-12}$ F m^{-1}), and S is the surface area of the active materials.

Gouy and Chapman have considered the reality of a diffused layer in the electrolyte resulting from the accumulation of ions on the surface of the electrode, as shown in Figure 5.2B. The potential decreases exponentially from the electrode surface to the electrolyte. Stern has integrated the Helmholtz and Gouy–Chapman

models into one model because the Helmholtz and Gouy–Chapman models are not sufficient to explain the actual phenomenon. The diffusion of ions in the electrolyte as well as the connection between the dipole moment of the electrolyte and active substance cannot be explained by the Helmholtz model.[6] In the Stern model, two ion distribution regions are involved: the diffusion layer (outside region) and Helmholtz layer,[6] as shown in Figure 5.2C. These two layers correspond to two series capacitors with capacitances of C_H (Helmholtz layer) and C_D (diffusion layer) contributing to the total capacitance of the electrode (C_{DL}), which can be evaluated by Eqn 5.2[5]:

$$\frac{1}{C_{DL}} = \frac{1}{C_H} + \frac{1}{C_D} \tag{5.2}$$

In order to provide the basis for the comparison between different electrode materials, it is a common practice to carry out galvanostatic charging-discharging (GCD) test. In a symmetrical system, the total capacitance (C, F g^{-1}) of the devices (two electrodes equal in mass, thickness, size, and materials) is calculation by Eqn 5.3:

$$C = 4\frac{It}{\Delta Vm} \tag{5.3}$$

where I (A) is the current, t (s) is the discharging time, ΔV (V) is the voltage window, and m (g) is the total mass of active materials. The stored specific energy E (Wh kg^{-1}) in a supercapacitor, also known as the energy density, is given by Eqn 5.4:

$$E = \frac{1}{2}CV^2 \tag{5.4}$$

where m (kg) is the mass of the supercapacitor and V is the maximum voltage window. Hence, a larger E can be achieved by increasing C or V. The maximum specific power (W kg^{-1}) also depends on the maximum voltage and is given by Eqn 5.5:

$$P = \frac{U_{max}^2}{4 \cdot ESR \cdot m} \tag{5.5}$$

where ESR (Ω) is the equivalent series resistance which is the sum of the ion resistance of the electrolyte impregnated in the separator, resistance of the electrode, and interface resistance between the electrode and current collector.

The pseudocapacitor is based on a Faradaic charging process in which the redox electron transfer process occurs on the electrode surface, as in the case of a battery. Unlike batteries, the capacitance stems from the formation of a specific relationship between the degree of charge acceptance and voltage change. The chemical reaction in pseudocapacitors is a fast and reversible process involving electron transfer, and the electrode materials do not undergo any phase change and not involve the creation or destruction of chemical bonds. Pseudocapacitors can provide a higher specific capacitance than EDLCs, thereby making them attractive to applications involving

large energy densities. The pseudocapacitance is given by the derivative of the charge stored (Δq) to the changing potential (ΔV) (Eqn 5.6):

$$C = \frac{d(\Delta q)}{d(\Delta V)} \tag{5.6}$$

Hybrid capacitors can achieve both high energy and power densities. The charge storage process depends on both the capacitive and Faraday characteristics such as ion adsorption and desorption at the electrode-electrolyte interface, reversible surface redox reactions on the electrode, and reversible reactions of the entire electrode.[7] The integration opens new opportunities for further improvement of energy storage and bridging the gap between batteries and EDLCs.

1.3 Supercapacitors

Supercapacitor cells have two different assembled structures, namely two-electrode cells and three-electrode cells. The two-electrode cells are used for research and commercial applications, while the three-electrode cells are mainly used for research because of their higher accuracy. The two-electrode cells consist of two electrodes, a metal current collector, and a separator. As for the three-electrode configuration, a reference electrode is added to make the measurement more accurate. Supercapacitor cells with the two and three-electrode configurations are schematically depicted in Figure 5.3A,B.[8]

1.3.1 EDLCs

EDLCs consist of two porous carbon-based materials as the electrodes, electrolyte, and separator. The charges stored are an electric double-layer electrostatic form and transferred between the electrode and electrolyte. Since the difference in potentials causes opposite charge attraction, there is no buildup of charges on the surface of the electrode when a voltage is applied. Inversely, electrolyte ions traverse the separator and diffuse to the oppositely charged electrodes, as shown in Figure 5.4A (EDLCs) which is illustrated with porous carbon.[9] The porous carbon with large SSA shortens the electrolyte ion transport channels and furthermore, the mechanism of EDLCs enables rapid energy adsorption and desorption, efficient energy transfer, and better power delivery.

1.3.2 Pseudocapacitors

The energy storage of pseudocapacitors involves three different mechanisms: adsorption-desorption (underpotential deposition), reduction oxidation (redox pseudocapacitor), and intercalation-deintercalation (intercalation pseudocapacitor).[11] The schematic diagram of a redox supercapacitor with metal oxide as the electrode and KOH as the electrolyte is shown in Figure 5.4B. When ions are inserted into the electrode, ion insertion occurs not only on the surface but also in the pores and layers of the redox active or conducting polymers. Furthermore, pseudocapacitive electrodes exhibit the capacitor-like behavior because their cyclic voltammograms resemble bilayer rectangles and linear hydrostatic discharge. Nonetheless, pseudocapacitors have a high capacity but

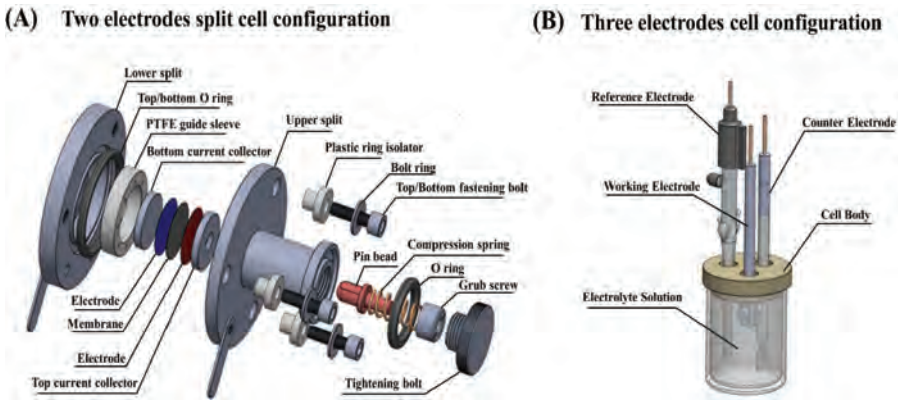

FIGURE 5.3 Schematic diagrams of two and three-electrode cells: (A) two-electrode configuration and (B) three-electrode configuration (reproduced with permission: Copyright 2022, Elsevier).[8]

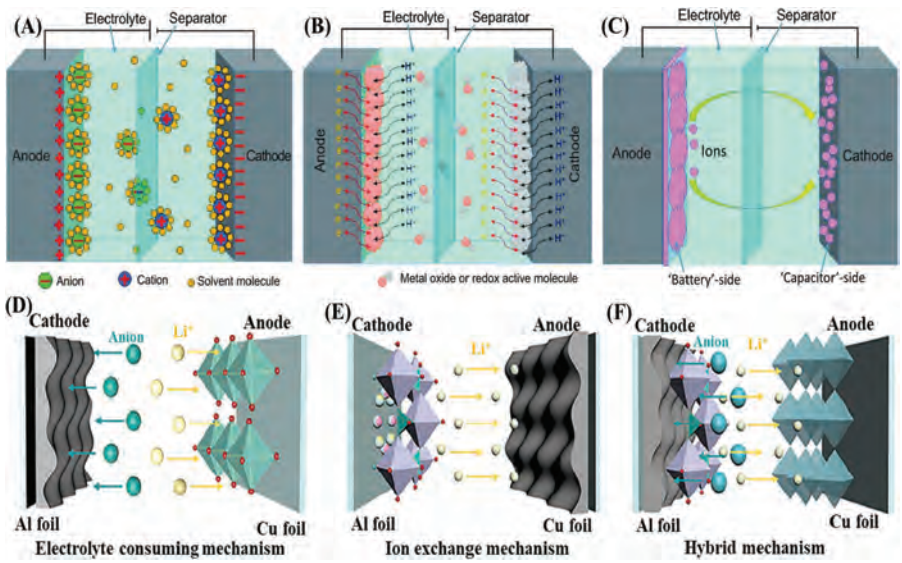

FIGURE 5.4 Schematic of the charge storage mechanisms: (A) EDLCs, (B) pseudocapacitors, and (C) battery-type electrodes (reproduced with permission: Copyright 2021, Elsevier)[9]; (D), (E), and (F) schematic of three energy storage mechanisms for MICs (reproduced with permission: Copyright 2021, Elsevier).[10]

poor stability and short cycling life due to the easy expansion and contraction during charging-discharging cycles. The active materials form defects due to the repeated insertion/extraction of redox-reactive ions on the surface of the active materials, leading to severe expansion and collapse of the electrode structure. Therefore, the cyclic stability of pseudocapacitors is slightly worse than that of EDLCs.

1.3.3 Metal-ion capacitors

Metal-ion capacitors (MICs) have been used in advanced hybrid electrochemical energy storage systems to solve the problems of low energy of capacitors and low power of LIBs. MICs consist of a battery-type anode (electrochemical insertion or conversion) and a capacitor-type cathode (physisorption) in an electrolyte containing metal ions, which have many characteristics of LIBs and SCs (Figure 5.4C). During charging and discharging, the cathode and anode undergo physical (adsorption/desorption) and chemical (intercalation/delamination or conversion) processes to store and release the energy, respectively. Due to the integration of two energy storage mechanisms in one device, MICs have several advantages including: (1) higher energy density than SCs; (2) higher power density than LIBs; (3) wider working temperature range from −50 to 85°C; and (4) better self-discharging performance than SCs.

Depending on whether the electrolyte is consumed during the electrochemical process, the energy storage mechanisms of MICs can be classified into three types: electrolyte consumption mechanisms, ion exchange mechanisms, and hybrid energy storage mechanisms[10]:

1. Electrolyte consumption mechanisms. In this system, the battery materials use alkali metal ion de/intercalation compounds as the anode (positive) and capacitive materials such as activated carbon, graphene, and carbon nanotubes extracted from biomass as the cathode (negative). During charging, the cations and anions move toward the anode and cathode electrodes, respectively, consistent with the mechanism of SCs. However, instead of physical adsorption, alkali metal ions can insert into the compounds containing alkali metal ions or undergo reduction reactions at the anode. During discharging, the alkali metal ions desorb from the anode back to the electrolyte, and the anions desorb from the cathode to reach charge equilibrium (Figure 5.4D).[10]
2. Ion exchange mechanisms. In this system, the cathode is the battery material that provides the alkali metal ions, while the anode is the capacitive material. During charging and discharging, the electrolyte concentration is kept constant and it only serves to transfer alkali metal ions, similar to a rocking chair-type alkali metal ion battery. Unlike the battery, the alkali metal ions are de-embedded from the cathode and adsorb on the anode surface when MICs are charged and vice versa (Figure 5.4E).
3. Hybrid energy storage mechanisms. The distinctive feature of these MICs is that one or both electrodes contain both the battery and capacitor materials. During charging, the all alkali metal ions are removed from the cathode into the electrolyte, and the alkali metal ions supplied by the electrolyte are inserted into the anode and vice versa (Figure 5.4F).

2 BIOMASS-DERIVED GRAPHENE-LIKE CARBON MATERIALS FOR SUPERCAPACITORS

Graphene-based materials are promising electrode materials for SCs on account of the large theoretical surface area, high electronic conductivity, and electrochemical stability. Nevertheless, their large-scale applications are often restricted by irreversible

aggregation and stacking caused by the strong van der Waals forces between the substrate surfaces of graphene nanosheets. This significantly restricts the diffusion pathways of ions within some narrow channels, thus preventing the electrolyte ions from entering the surface of the graphene nanosheets, leading to a significant loss of the ion-accessible surfaces and making the specific capacitance much smaller than the theoretical value (ca. 550 F g^{-1}).[12] BDGC materials are an effective solution because they have a large surface area, porous structure, high graphitization degree, and chemically stable surface by controlling the preparation method. What's more, BDGC materials have interconnected pore networks, good electrical conductivity, and electrochemically stable surface boding well for SCs.

2.1 Chemical composition of biomass

The chemical components in biomass are covalently bonded carbohydrate monomers which consist of starch, lignocellulose, triglycerides, phenols, terpenes, fatty acids, and trace amounts of iron, calcium, potassium, silicon, and other elements.[11] For example, lignocellulosic biomass consists of mainly cellulose, hemicellulose, and lignin (Figure 5.5).[11, 13] There is also biomass composed of carbon, hydrogen, and oxygen together with trace amounts of nitrogen, sulfur, and phosphorus. The components in plant-based biomass can be converted into carbon by heat treatment or carbonization. The components in lignocellulose interact strongly with covalent or noncovalent forces. Cellulose is a linear polysaccharide consisting of a large molecular weight D-glucose linked uniformly by a β-1-4 glucosidic bond and accounts for 40%–50% of lignocellulosic biomass.[13] Hemicellulose with branching and amorphous characteristics as well as a small degree of polymerization makes up 25%–35% of the total biomass. Thus, hemicellulose tends to decompose thermally. Lignin is a component in lignocellulosic biomass and amorphous polymers accounting for 15%–20% of the biomass. In addition, lignin has a number of aromatic functional groups consisting of p-coumarol, pinacol, and sinapyl alcohol.

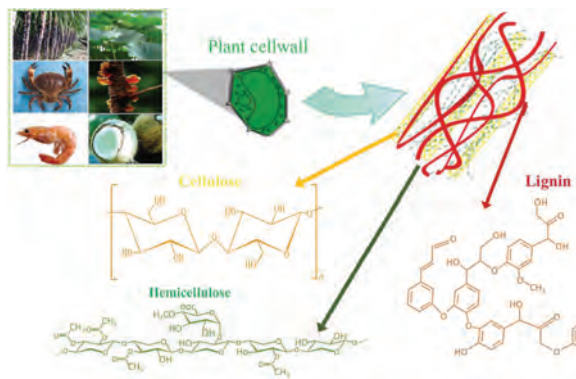

FIGURE 5.5 Structure of lignocellulosic biomass (reproduced with permission: Copyright 2023, Elsevier).[11]

2.2 Graphene-like carbon materials derived from biomass

The biomass mainly composed of cellulose and hemicellulose is broadly found on earth and can be used to synthesize porous carbon due to the unique natural structure as well as high carbon and low ash contents. Graphene-like carbon (GLC) produced from biomass generally has a porous structure that provides connectivity for different pore sizes, shortens the ion pathways, and lowers the resistance in ion transport. For example, coconut shells can easily be converted into porous GLCs by a chemical treatment with $ZnCl_2$ and $FeCl_3$ activation.[14] The resulting GLCs have a large SSA (1,874 $m^2 g^{-1}$) and high graphitization degree ($I_G/I_D \approx 1.81$). The carbon atoms with sp^2 covalent bonds provide high electrical conductivity to reduce the resistance of the system. Similarly, three-dimensional GLCs (3D GLCs) with graphene-like sheets, large SSA (1,503 $m^2 g^{-1}$), and high electrical conductivity (32.14 S cm^{-1}) formed from coconut shells can be obtained by K_2CO_3 catalytic graphitization.[15] SEM shows that the honeycomb-like structure is composed of ultrathin graphene sheets (Figure 5.6A) and well-developed interconnected pores and pore sizes in the range of micrometers (Figure 5.6B). The graphene nanosheets are curved and wrinkled and composed of about three to four layers, as revealed by TEM. The Raman spectrum of 3D GLCs shows low-intensity D-band, sharp G–band, and 2D-band, with an $I_{D/G}$ of only 0.088, while the ratio of $I_{2D/G}$ is as high as 0.855 (Figure 5.6C) confirming high-quality graphene sheets. Hence, 3D GLCs have outstanding electrochemical properties. Without conductive additives, the capacitance of 3D GLCs is 91.15 F g^{-1} at 0.2 A g^{-1} and retention is 85.1% after 5,000 cycles at 0.1 A g^{-1} in an organic electrolyte.

The nitrogen-doped (N-doped) GLC nanosheets from pine nut shells can be obtained by combination with melamine and KOH activation. The GLCs are composed of ultrathin nanosheets and irregular nanosheets and the thickness of the nanosheets is about 5–8 nm (Figure 5.6D–E).[16] The GLC nanosheets have outstanding electrochemical properties due to the large SSA (2,090 $m^2 g^{-1}$) and the inherent hierarchical porous sheets structure. Hence, the GLCs exhibit a superior specific capacitance of 324 F g^{-1} at 0.05 A g^{-1}, high rate capacitance of 258 F g^{-1} at 20 A g^{-1}, and excellent cyclic stability of 94.6% after 10,000 cycles at 2 A g^{-1} in 6 M KOH (Figure 5.6F).

2.2.1 GLCs from forest plants and residues

The preparation of BDGCs from forest plants and residues by different activations provides a green and economical possibility for developing 2D carbon or 3D skeleton carbon consisting of 2D carbon nanosheets. For instance, porous GLC sheets with an ultrathin thickness (3.8 nm) and a hierarchically porous structure with a large meso-pore ratio from pine bark can be obtained by potassium acetate activation (Figure 5.7A).[17] The GLC sheets have a high capacitance (128.1 F g^{-1} at 1 A g^{-1}), good cycling stability, and satisfactory energy density (32.4 Wh kg^{-1}) and power density (30.375 kW kg^{-1}) in the $TEABF_4$/AN electrolyte.[17] Similarly, GLCs with large amounts of interconnected nanosheets with a thickness of 10 nm and large SSA (979.89 $m^2 g^{-1}$) are prepared from Enteromorpha by high-temperature melting of K_2CO_3 (Figure 5.7B).[18] The GLCs have wide pore distributions and a suitable

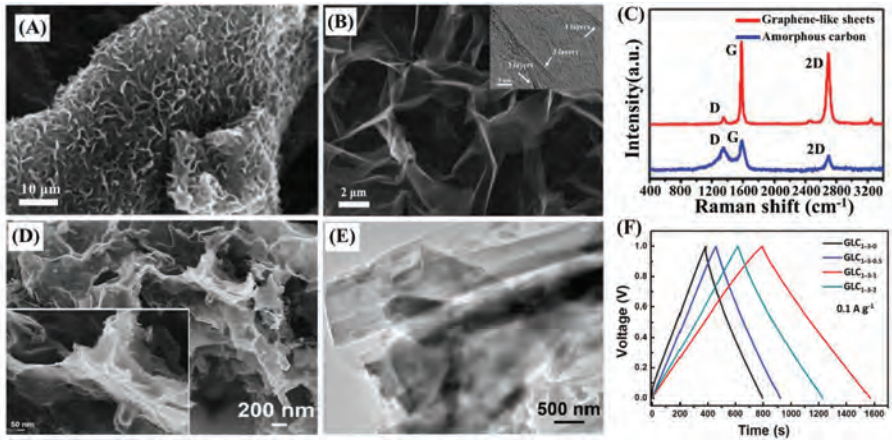

FIGURE 5.6 (A) SEM image and (B) enlarged SEM image; (C) Raman scattering spectra of 3D GLCs (reproduced with permission: Copyright 2018, Royal Society of Chemistry)[15]; (D) SEM image, (E) TEM image, and (F) GCD curves of GLC nanosheets from pine nut shells (reproduced with permission: Copyright 2019, American Chemical Society).[16]

amount of oxygen, thus enabling the electrolyte ions to enter the surface and interior of the electrode (Figure 5.7C). In addition, the GLC nanosheets with abundant porosity, well-developed porous structure, large SSA, and high conductivity are prepared from fresh lotus receptacles by "drilling" holes with H_2O_2 and exfoliating into graphene-like nanosheets with HAc, followed by carbonization (Figure 5.7D).[19] The GLC nanosheets have very high specific capacitance (340 F g^{-1} at 0.5 A g^{-1}), large capacitance retention of 98% after 10,000 cycles, and outstanding energy density (23.33 Wh kg^{-1}).

3D GLCs with the 3D interconnected graphene nanosheet structure can be prepared from spruce bark hydrothermally and KOH activation (Figure 5.7E).[12] The 3D GLCs are composed of intertwined vertically aligned graphene nanosheets, which link to each other and form a 3D honeycomb-like structure to offer porous space between the contiguous layers (Figure 5.7F). The Raman spectrum of 3D GLCs shows low-intensity D-band, sharp G-band, and 2D-band at around 1,350 cm^{-1}, 1,584 cm^{-1} and 2,700 cm^{-1} (Figure 5.7G). The 2D band is a feature of the two-phonon resonance second order, and its width and position are sensitive to the number of layers in the graphene sheet. For instance, single-layered graphene displays a sharp 2D peak, while two-layered graphene shows a relatively wide 2D band. The D peak at 1,350 cm^{-1} is attributed to carbon atom breathing vibration which is related to the six-membered sp^2 carbon rings. The D peak indicates the existence of defects in the materials, which are absent from defect-free graphene. The intensity ratio of the G- and D-band (I_G/I_D) is used to measure the defects in materials. The 3D GLCs possess a 3D interconnected structure, large SSA (2,385 $m^2 g^{-1}$), many hierarchical pores (1.68 $cm^3 g^{-1}$), and open surfaces with graphene nanosheets, thus showing an outstanding capacitance of 239 F g^{-1} at 1 A g^{-1} and high energy density of 74.4 Wh kg^{-1} in the $TEABF_4$/AN electrolyte.

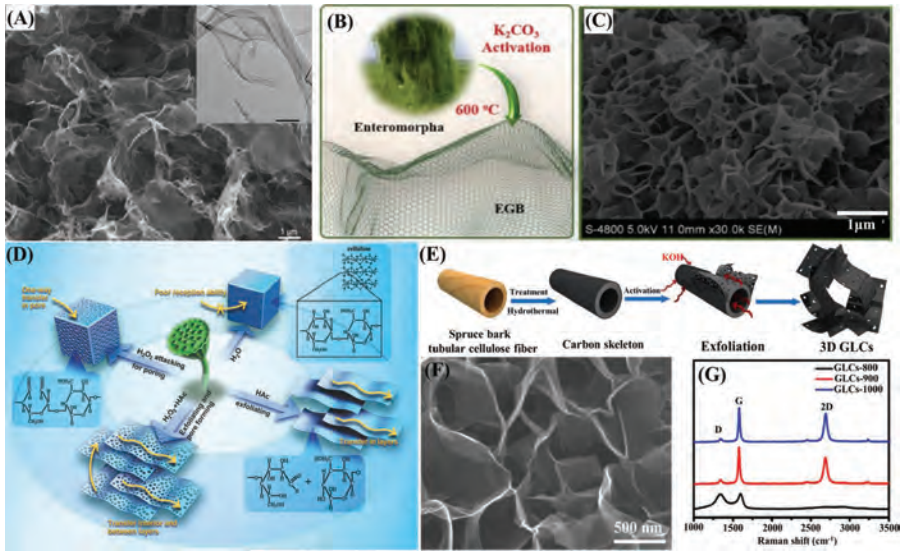

FIGURE 5.7 (A) SEM and TEM (inset) images of GLCs (reproduced with permission: Copyright 2019, American Chemical Society)[17]; (B) preparation of GLCs from Enteromorpha, (C) SEM image of GLCs (reproduced with permission: Copyright 2020, Elsevier)[18]; (D) preparation process of GLC nanosheets from the lotus receptacle (reproduced with permission: Copyright 2017, Wiley-VCH Verlag)[19]; (E) preparation of 3D GLCs from spruce bark, (F) SEM image and (G) Raman scattering spectra of 3D GLCs (reproduced with permission: Copyright 2017, Elsevier).[12]

2.2.2 GLCs from agricultural products

The preparation of high-quality GLC materials from agricultural products for SCs has advantages such as the low cost, abundant raw materials, and sustainable nature. For example, GLC nanosheets can be prepared from hemp bast fibers by hydrothermal carbonization and KOH activation (Figure 5.8A).[20] The GLC nanosheets are made of highly interconnected carbon and ultrathin carbon nanosheets (10–30 nm in thickness) and have high meso-porosity (58%). Hence, the GLC nanosheets with a large SSA (2,287 $m^2 g^{-1}$) and electrical conductivity (226 S m^{-1}) show a high specific capacitance of 142 F g^{-1} with excellent capacitance retention as well as a high energy density of 19 Wh kg^{-1} in the ionic liquid electrolyte. Similarly, the porous GLCs are prepared from fungus by hydrothermal treatment in KOH and carbonization (Figure 5.8B).[21] The porous GLCs with a hierarchically interconnected porous framework and wide pore distributions have a large SSA (1,103 $m^2 g^{-1}$) and bulk density (0.96 g cm^{-3}) thus providing more storage sites and shorter transport paths for the electrolyte ions. As a result, the porous GLCs exhibit a high volumetric capacitance of 360 F cm^{-3} and retention of 99% after 10,000 cycles. The N-doped porous GLC sheets formed from layered peanut seed coats with triethanolamine by thermal exfoliation and pyrolysis have graphene-like sheets with a thickness of ~4 nm and large SSA (887 $m^2 g^{-1}$), which improve the electrical conductivity (8.1 S cm^{-1}) and wettability (Figure 5.8C).[22] Consequently, the GLC sheets show ultra-high rate capabilities

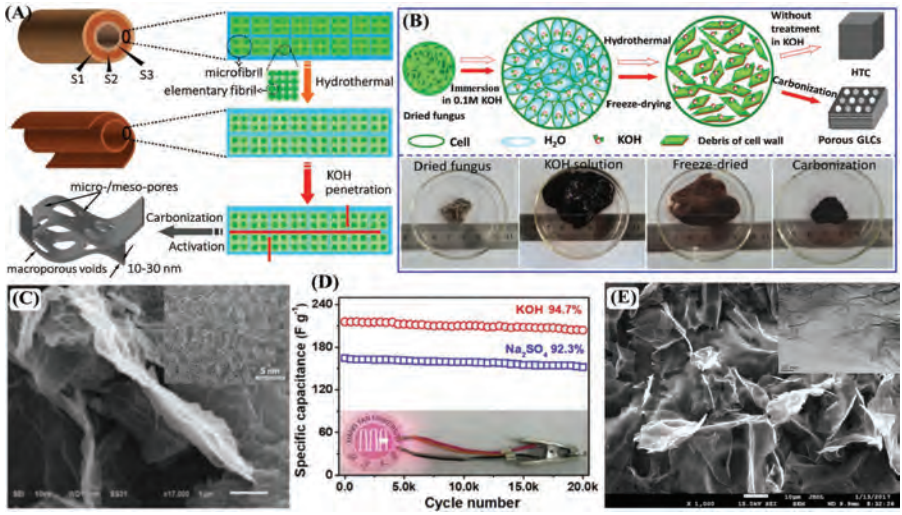

FIGURE 5.8 (A) Preparation of GLCs from hemp (reproduced with permission: Copyright 2013 American Chemical Society)[20]; (B) preparation of porous GLCs from fungus (reproduced with permission: Copyright 2015, Elsevier)[21]; (C) SEM and HR-TEM (inset) images of the porous GLC sheets, (D) cycling stability of the porous GLC sheets (reproduced with permission: Copyright 2020, Elsevier)[22]; (E) SEM image of the porous GLCs formed from sugarcane bagasse pith (reproduced with permission: Copyright 2017, Elsevier).[23]

(72.5% capacity at 200 A g^{-1}) and cycling stability (92.3% of capacity retention after 20,000 cycles at 10 A g^{-1}) in 6.0 M KOH and 1 M Na_2SO_4 electrolytes, respectively (Figure 5.8D). Similarly, the N-doped porous GLC sheets synthesized by KOH activation (Figure 5.8E)[23] have a large-size multiscale wrinkled nanosheet structure, large SSA (1,786.1 $m^2 g^{-1}$), and appropriate amount of N. The N-doped GLC sheets show a large specific capacitance (339 F g^{-1} at 0.25 A g^{-1}), long-term cycling stability (97.9% capacitance retention after 10,000 cycles), and high energy density (11.77 Wh kg^{-1}) in 6 M KOH.[24]

2.2.3 GLCs from marine sources

Marine products are abundant and produced from the ocean that can be eaten or used such as fish, shellfish, and raw plants (seaweed, nori, kelp, etc.). Shellfish mainly includes crab, shrimp, lobster shells, and oysters. Shellfish harbors useful proteins, calcium carbonate, and chitin. Chitin is a linear polymer (poly b-(1, 4)-*N*-acetyl-D-glucosamine) containing nitrogen, which is the second most abundant natural biopolymer on earth (after cellulose).[25] Shellfish is a renewable porous carbon precursor for the direct preparation of graphene carbon nanosheets with N dopant and tunable porosity.

The N-doped GLC sheets are prepared from naturally layered shrimp shells by simultaneous carbonization and auto-activation followed through ultrasonic liquid exfoliation (Figure 5.9A).[26] The GLC sheets possess the graphene sheet structure (5 nm thickness), large SSA (1,946 $m^2 g^{-1}$), and big nitrogen content (8.75 wt%) for

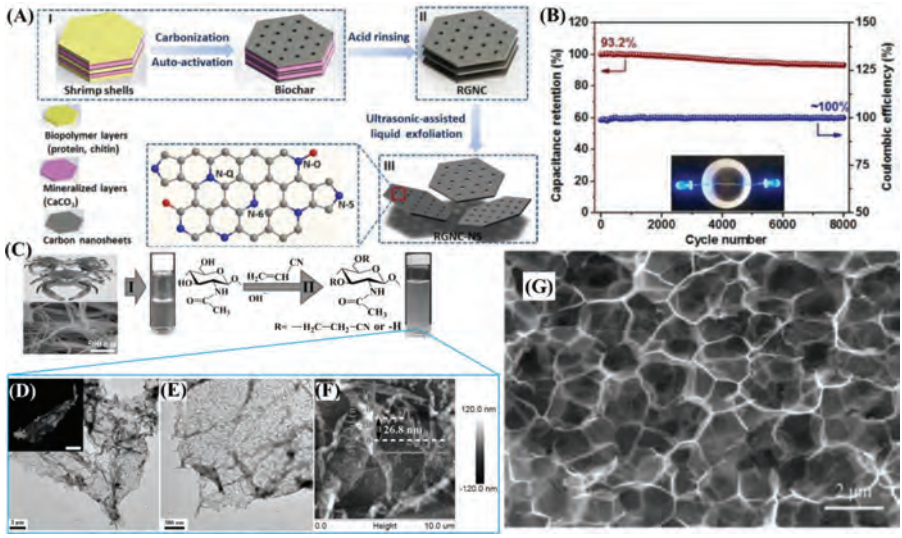

FIGURE 5.9 (A) Synthetic pathway of N-doped GLC sheets; (B) cyclic stability (two blue LEDs in inset) of N-doped GLC sheets (reproduced with permission: 2016, Royal Society of Chemistry)[26]; (C) synthetic pathway and microscopic of GLC sheets, (D and E) TEM and (F) AFM images of GLC sheets (reproduced with permission: 2017 WILEY-VCH Verlag GmbH & Co. KGaA, Weinheim)[27]; (G) SEM images of N-doped GLCs (reproduced with permission: 2016, Royal Society of Chemistry).[28]

improved conductivity (7.8 S cm^{-1}) and wettability with the electrolyte. The GLC sheets have an excellent rate capability with a high capacitance of 322 F g^{-1} at 0.5 A g^{-1}, long cyclic stability (93.2% capacitance retention after 20,000 cycles), and high energy-power density (30 Wh kg^{-1} and 64,000 W kg^{-1}) in ionic liquid electrolytes (Figure 5.9B). Similarly, the N-doped porous GLC sheets formed from chitosan show a large SSA of 1,321.3 m^2g^{-1}, large pore volume of 4.21 cm^3g^{-1}, ultrathin nanosheets structure, and appropriate porosity.[29] The GLC sheets with a thickness of 27 nm are fabricated from crab chitin *via* hydrophobization-induced interfacial assembly followed by the aqueous NaOH/urea treatment (Figure 5.9C).[27] The layers possess structural flexibility and robustness, thin chitin nanosheets (26.8 nm), and a large SSA of 724.2 m^2g^{-1} (Figure 5.9D–F). When the hybrid films of chitin and GLC sheets are used in the flexible device, the ultrathin soft film has a good specific capacitance of 162.4 F g^{-1} at 0.5 A g^{-1} and high cycling stability (capacity retention up to 95% after 10,000 cycles at 5 A g^{-1}) in 6 M KOH. In addition, the 3D honeycomb-like N-doped GLC films formed by mixing chitin and graphene oxide are synthesized by dissolution and coagulation of chitin and graphene oxide in the NaOH/urea aqueous solution using a repeated freezing-thawing process followed by carbonization under Ar.[28] The honeycomb-like N-doped GLC films have a homogeneous interconnected open-cell framework with the average pore size of about 2 μm (Figure 5.9G). The porous N-doped GLC films inherit the high conductivity of graphene and have abundant porosity and rich active sites resulting in excellent electrochemical properties.

2.3 Biomass-derived carbon-based composites

Compared to pure carbon materials, pseudocapacitor materials are based on transition metal oxides or hydroxides, such as MnO_2, Fe_2O_3, Co_2O_3, and $Ni(OH)_2$, which have high capacity and good redox activity. The redox activity of the materials is mainly derived from the multivalent nature of the transition metals. However, the poor inherent conductivity and small SSA lead to a slow charge transfer and suboptimal cycling stability at high current densities.

BDGCs can provide abundant space for the deposition of transition metal oxides or hydroxides and reduced agglomeration. The superior electrical conductivity of BDGCs can expedite charge transfer to improve the electrochemical performance. In addition, the good structural stability and proper porous structure of BDGCs can buffer the volume expansion caused by transition metal oxides or hydroxides. Therefore, the combination of transition metal oxides or hydroxides with BDGCs improves the electrochemical properties. For example, the multifunctional heteroatom (Fe, N, S) Co-doped GLC sheets (Fe-N-S/GLC) with special 2D layer structures are formed from silkworm chrysalides shells by liquid-phase exfoliation to delaminate the multilayered biochars (Figure 5.10A).[30] Owing to the unique integration of the graphene-like structures with a thickness of 4.3 nm, large SSA (2,491 $m^2 g^{-1}$), hierarchical pores, homogenous co-doping, and high electronic conductivity (7.6 S cm^{-1}), the Fe-N-S/GLC sheets have excellent super-capacitive properties such as a large capacitance of 173 F g^{-1} at 1 A g^{-1} and energy density of 29.1 Wh kg^{-1} in an ionic liquid electrolyte.

$Ni(OH)_2$ is an attractive material for SCs due to the high theoretical specific capacitance (2,358 F g^{-1}), specific redox behavior, high redox activity, and environmental friendliness. However, the inherently low electrical conductivity (10^{-17} S cm^{-1}) of $Ni(OH)_2$ leads to redox reactions occurring only on the surface and low utilization. To overcome these problems, $Ni(OH)_2$ is combined with GLCs to enhance the electrochemical performance. In this respect, GLCs with the nanosheet-like structure formed from peach gum with $Ni(OH)_2$ to $Ni(OH)_2$/GLCs have excellent electrochemical properties (Figure 5.10B).[31] In the process, GLCs are first obtained by hydrothermal carbonization and magnesium acetate activation to form $Ni(OH)_2$. The synergistic effects of $Ni(OH)_2$ and GLCs produce $Ni(OH)_2$/GLCs with a large energy density of 36.9 Wh kg^{-1} and power density of 400 W kg^{-1}.

Other pseudocapacitive materials, such as MnO_2, Co_3O_4, Fe_2O_3, NiO, and $NiMn_2O_4$ can also be combined with GLCs to promote capacitance. The N-doped 3D porous GLCs (3DPGLCs) are formed from luffa complexes with $NiMn_2O_4$ nanocrystals ($NiMn_2O_4$/3DPGLCs) by carbonization and a hydrothermal method to form an efficient binder-free electrode (Figure 5.10C).[32] The 3DPGLCs with a porous structure and defective surface can adjust *in situ* growth of $NiMn_2O_4$ to form the $NiMn_2O_4$/3DPGLCs composite. Because the $NiMn_2O_4$/3DPGLCs composite has a high conductive network and abundant pores, it not only is conducive to electrolyte and $NiMn_2O_4$ infiltration but also transfers electrons quickly for the electrochemical reaction. The $NiMn_2O_4$/3DPGLCs electrode has a high specific capacitance of 1,308.2 F g^{-1} at 1 A g^{-1} and rate performance of 77.9% at 15 A g^{-1}. The GLCs formed from cleaned agaric are combined with MnO_2 nanosheets (MnO_2/GLCs) by a

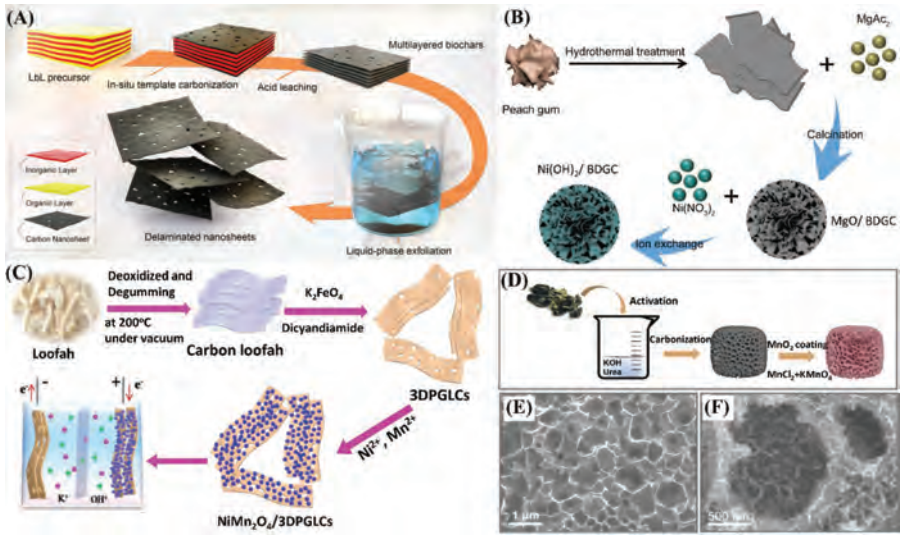

FIGURE 5.10 (A) Preparation of the Fe-N-S/GLC sheets (reproduced with permission: Copyright 2021, Elsevier)[30]; (B) preparation of $Ni(OH)_2$/GLCs composites (reproduced with permission: Copyright 2019, Elsevier)[31]; (C) preparation of $NiMn_2O_4$/3DPGLCs (reproduced with permission: Copyright 2020, Elsevier)[32]; (D) schematic diagram of the MnO_2/N-GLCs composite. (E) SEM image of GLCs; (F) SEM image of the MnO_2/GLCs composite (reproduced with permission: Copyright 2020, Elsevier).[33]

two-step process (Figure 5.10D).[33] The first step consists of a direct heat treatment of the cleaned agaric and KOH activation is performed to obtain the GLCs. The second step includes *in situ* chemical deposition and dense MnO_2 nanosheets are grown on porous carbon (Figure 5.10E,F). The conductive frame of the N-doped porous carbon and synergetic effects between GLCs and MnO_2 yields MnO_2/GLCs with a large SSA (2,250 $m^2 g^{-1}$) produce excellent electrochemical performance such as a specific capacitance of 330 F g^{-1} at 1 A g^{-1}. Similarly, the GLC sheets are formed from salvia splendens petals coupled with MnO_2 (MnO_2/GLCs) by carbonization and hydrothermal processes.[34] The MnO_2/GLCs composite possesses a large SSA (483 $m^2 g^{-1}$) and suitable pore size distribution (2–5 nm). Because of the synergistic effects of MnO_2 and GLC, the MnO_2/GLCs composite electrode shows a high specific capacitance of 438 F g^{-1} at 0.5 A g^{-1} and large rate capability (67.8% capacity at 50 A g^{-1}) in the Na_2SO_4 electrolyte. The composites containing different GLCs and transition metal oxides or hydroxides are prepared from kapok fiber/NiO, fruit/Co_3O_4, and wheat straw/Fe_2O_3 and have been used as electrode materials in SCs.

3 PREPARATION METHODS OF GLCS FROM BIOMASS

In this section, the preparation of graphene-like materials from biomass is classified into physical activation, chemical activation, microwave-assisted activation, template method, and other methods.

3.1 Physical activation

Physical activation mainly utilizes water steam and CO_2 as the activators to prepare BDGCs. The common preparation process involves carbonization at 400–800°C followed by activation at 700–1,500°C, using the chemical reactions between carbon and H_2O (Eqn 5.7) or CO_2 (Eqn 5.8)[35]:

$$C+H_2O \rightarrow H_2+C \quad H = +132 \text{ kJ mol}^{-1} \tag{5.7}$$

$$C+CO_2 \rightarrow 2CO \quad H = +173 \text{ kJ mol}^{-1} \tag{5.8}$$

The activation process involves the controlled combustion of activated carbon atoms and the elimination of volatile species. The quality of GLCs depends on the conditions, such as temperature, time, gas flow rate, and activator. In addition, the different biomass materials require the appropriate activators to obtain GLCs with large SSA and suitable pores. For instance, GLCs with SSA of 1,700 $m^2 g^{-1}$ and pore volume of 1.135 $cm^3 g^{-1}$ are prepared from coconut shell char by CO_2 activation.[36] In addition to CO_2 activation, water steam is widely used as an effective activator due to its low cost, cleanliness, and safety. For example, GLCs prepared from shrimp shells by water steam activation at 900°C show an SSA of 560.6 $m^2 g^{-1}$ and a high degree of graphitization (I_D/I_G=0.7686).[37]

3.2 Chemical activation

Chemical activation is a process in which the precursor is first mixed with certain chemicals and then activated to obtain BDGCs at a temperature of 500–1,000°C. Compared to physical activation, chemical activation has several advantages[38]: (i) The pores are well developed; (ii) The activation time is shorter; (iii) GLCs have large SSA; (iv) There is a high degree of graphitization. Various activating regents have been used, for instance, KOH, NaOH, H_3PO_4, $ZnCl_2$, $FeCl_3$, and K_2CO_3. KOH is a popular alkali activator that produces the best effects. The specific reactions are as follows (Eqns 5.9–5.13)[39]:

$$6KOH+2C \leftrightarrow 2K+2K_2CO_3+3H_2 \tag{5.9}$$

$$K_2CO_3 \leftrightarrow K_2O+CO_2 \tag{5.10}$$

$$K_2CO_3+2C \leftrightarrow 2K+3CO \tag{5.11}$$

$$K_2O+C \leftrightarrow 2K+CO \tag{5.12}$$

$$CO_2+C \rightarrow 2CO \tag{5.13}$$

In the chemical activation stage, the pores are developed with the consumption or redevelopment of carbon. KOH reacts with carbon to form metallic K, K_2CO_3, and

H_2 gas at a temperature lower than 570°C (Eqn 5.9). K_2CO_3 is decomposed to form K_2O and CO_2 pyrolysis occurs at around 600°C (Eqn 5.10). KOH is completely consumed at 700°C. K_2CO_3 and K_2O start to decompose and are absent from the system at above 800°C (Eqns 5.11 and 5.12).[38] The activated products of CO_2 may also take part in the pore-forming process due to the physical activation effects. The produced CO_2 reacts with carbon to produce CO at a high temperature (Eqn 5.13). At a higher activation temperature (>750°C, Eqns 5.9–5.11), almost all the biochar is activated by the reaction between KOH and carbon. The K^+ diffuses into the interior of the carbon skeleton to expand or create new pores during the activation process.

Different types of biomass have different SSA, pore volume, and degree of graphitization after chemical activation. For example, the GLC sheets formed from gelatin by KOH activation have a large SSA of 3,106 $m^2 g^{-1}$, pore volume of 1.70 $cm^3 g^{-1}$, and thin sheets of graphene.[40] The N-doped hierarchical porous GLCs aerogels formed from chitosan by carbonization at 800°C and KOH activation have large SSA of 2,435.2 $m^2 g^{-1}$ and pore volume of 1.65 $cm^3 g^{-1}$.[41] Other GLCs such as petroleum pitch (2,132 $m^2 g^{-1}$) and sorghum (4,092 $m^2 g^{-1}$) also have enhanced SSA after KOH activation.

Compared to KOH, NaOH activation has the preponderant in terms of merits such as less corrosion, lower weight dosage, and low cost. NaOH is also extensively employed to fabricate porous GLCs. NaOH reacts with carbon to form pores and the enlargement increases graphitization in the product. There are some possible reactions between the reactive intermediates and carbon surface producing H_2, CO_2, and CO, which give rise to the development of pores according to the following equations (Eqns 5.14–5.18)[42]:

$$6NaOH+2C \leftrightarrow 2Na+2Na_2CO_3+3H_2 \tag{5.14}$$

$$Na_2CO_3 \leftrightarrow Na_2O + CO_2 \tag{5.15}$$

$$Na_2CO_3+2C \leftrightarrow 2Na+3CO \tag{5.16}$$

$$Na_2O+C \leftrightarrow 2Na+CO \tag{5.17}$$

$$CO_2+C \rightarrow 2CO \tag{5.18}$$

For example, GLCs obtained from chitin by NaOH activation at 800°C show a large SSA of 294 $m^2 g^{-1}$ and a pore size of 25 nm.[43] Similarly, GLCs obtained from guava seeds have a large SSA of 2,573.6 $m^2 g^{-1}$ and a total pore volume of 1.260 $cm^3 g^{-1}$ after NaOH activation.[44]

3.3 Microwave-assisted activation

Microwave-assisted activation is a new technology for the construction of BDGCs. In the microwave system, heat is generated within the substance. The microwave transmitted to biological tissues causes molecules and polar side chains of proteins to oscillate at high frequencies due to electromagnetic oscillations of molecules and

high-speed molecular motion, leading to the generation of heat.[45] The heat on the molecular level increases the temperature rapidly and uniformly, which is not possible by conventional heating. Therefore, microwave-induced activation is carried out in a closed space, thus solving most of the problems associated with conventional pyrolytic activation, consequently giving rise to higher efficiency, resource saving, shorter cycles, and low costs. Li et al. have combined microwave heating and steam activation to extract high-quality porous GLC nanosheets from black sesame.[46] The GLC nanosheets have high and uniform porosity, large SSA (2,414.5 $m^2 g^{-1}$), and a high degree of graphitization. In short, owing to the many advantages offered by microwave-induced physical activation, it has been used to prepare GLCs with some good results.

3.4 Template methods

Template synthesis is one of the effective methods to fabricate porous BDGCs with controlled structures and higher efficiency. In this technique, the template simply acts as a bracket around which the other types of materials are synthesized. The template reacts with the carbon precursor to increase the degree of graphitization of the carbon structure during carbonization and then removes the template with chemicals or heating to guide pore formation. Currently, the two types of templates are hard templates and soft templates.

Hard templates, such as MgO, $CaCO_3$, ZnO, Fe_2O_3, and SiO_2 are commonly used to fabricate porous structures of GLCs. The structural features of porous GLCs prepared from hard templates depend on the physical/chemical properties of the template. The preparation of porous GLCs by the hard template method involves four steps: (i) synthesis of the ideal hard template; (ii) effective mixing of carbon sources and template; (iii) high-temperature pyrolysis under certain atmosphere, and (iv) hard template removal by acid or alkali rinsing.[47] For instance, corrugated GLC nanosheets prepared from tar pitch with the plate-like MgO template followed by KOH activation have a large SSA of 2,132 $m^2 g^{-1}$ and pore volume of 1.23 $cm^3 g^{-1}$. Corrugated GLC nanosheets have micropores, mesopores, and macropores with a controllable pore size distribution.[48]

ZnO templates have received much attention due to their unique physicochemical properties. The carbon precursors tend to react with ZnO and produce gases during high-temperature processing, which plays a role in physical activation. ZnO has the bifunctional hard templating and physical activation and the GLCs with well-developed porous structures and wide pore size distributions can be obtained. For example, 3D flower-like and hierarchical of GLCs are obtained from pitch with a ZnO template and chemical activation. The GLCs have not only 3D interconnected porous graphene sheets and wide pore size distribution but also a large SSA of 761.5 $m^2 g^{-1}$ and total pore volume of 0.49 $cm^3 g^{-1}$.[49] Compared to MgO and ZnO, $CaCO_3$ is a reliable template and this kind of dual template is used to prepare GLCs. $CaCO_3$ preferentially decomposes to form CaO particles and CO_2 gas at 500°C. The generated CO_2 gas is a reactant with carbon to produce different porous structures. When CaO is removed, hierarchical porous GLCs are formed. For instance, hierarchical porous GLCs with an interconnected pore structure are obtained from cornstalk without

pith using the $CaCO_3$ template and $K_2C_2O_4$ activation. The hierarchical porous GLCs have a large SSA (1,910 $m^2 g^{-1}$) and well-developed hierarchical porosity.[50]

Soft templates are also effective in constructing graphene. They are usually organic molecules or super-molecules with functional groups. In certain solvents, the functional groups of the soft templates can provide hydrogen bonding, hydrophobic and hydrophilic interactions, and electrostatic interactions. When a suitable solvent is added, the soft template becomes micelles that interact with the molecules in the carbon precursors. During carbonization, the micelles break down to form the carbon source and biomass charcoal to produce GLCs with a unique porous structure. The 3D interconnected porous GLCs are synthesized using cheap coal tar pitch as the carbon source, $BMIMBF_4$ ionic liquid as the soft template, and KOH activation.[51] The 3D GLCs composed of thin carbon nanosheets with well-developed pores possess a large SSA of 1,593 $m^2 g^{-1}$ and a total pore volume of 0.85 $cm^3 g^{-1}$.

3.5 Other methods

Other activation methods like hydrothermal carbonization, salt-based method, and physicochemical activation have also been applied to the preparation of BDGCs. The BDGCs with well-developed and interconnected porous structures are formed from natural reed membranes by hydrothermal and carbonization treatments.[52] The BDGCs with a hierarchical porosity and graphene structure formed from kitchen waste hydrolyzed residues with NaCl–KCl molten salts at 800°C have a large SSA (818.65 $m^2 g^{-1}$).[53] Self-activation allows the conversion of biomass to BDGCs without additional activators, since biomass has inherent inorganic salts or other metal ions (K, Na, Fe, and Ca) that can etch the carbonization precursors or react with gases emitted during carbonization (CO_2, H_2O, and H_2). This self-activating pathway has been applied to the preparation of BDGCs from coconut shells, almond kernels, and wood chips.

4 CONCLUSIONS AND OUTLOOK

BDGC is a promising electrode material in energy storage applications due to its abundant natural resources, renewability, low cost, adjustable porous structure, and good physicochemical stability. The rational design and preparation of BDGCs with adjustable SSA, pores, surface chemistry, and degree of graphitization are important for the application in SCs. The quality and performance of the BDGCs depend on the precursors and fabrication techniques. Although various biomass feedstock precursors used for physical activation, chemical activation, microwave-assisted activation, and template methods for the synthesis of BDGC have great potential for SCs, there are still some challenges for practical applications.

First, the carbon source plays an important role in the quality of the BDGC materials. Therefore, it is imperative to establish a unified technical standard or grading system for the carbon source. Second, comprehensive and standardized characterization methods should be established to evaluate the microscopic morphology of BDGC. Specifically, each 3D graphene structure has a unique structure and sheet

quality. Although the 3D structures are typically characterized by SEM, TEM, and AFM, some features pertaining to the microstructure of BDGC materials are still not well understood. Third, a standardized protocol is needed to determine the conductivity. The total conductivity should be calculated based on the actual cross-sectional area for a more reliable comparison. Alternatively, at least detailed information about the mass density and the actual contact area should be provided. Fourth, the relationship between the 3D microstructure of graphene and its main properties is not well understood. In practical applications, a database containing information about the structure and properties of various 3D graphene structures should be established. Such a database will allow not only systematic analysis and comparison of different 3D graphene structures but also easy selection of the proper 3D graphene structures for special applications.

In addition to the aforementioned challenges, the application of BDGC should be expanded. The diversity of biomass in terms of resource, type, structure, and composition bodes well for a wide range of applications including rechargeable batteries, desalination, catalysts, and oil/water separation. For example, BDGC materials with a large SSA, suitable pore size, and pore size distribution are desirable for seawater desalination, water treatment, and oil-water separation. Furthermore, these materials can be used as catalysts or substrates in metal-based catalytic applications.

REFERENCES

1. W. Zuo, R. Li, C. Zhou, Y. Li, J. Xia and J. Liu, Battery-supercapacitor hybrid devices: Recent progress and future prospects, *Adv. Sci*., 2017, **4** (7), 1600539.
2. L. Sun, Y. Gong, D. Li and C. Pan, Biomass-derived porous carbon materials: Synthesis, designing, and applications for supercapacitors, *Green Chem*., 2022, **24** (10), 3864–3894.
3. M. Athanasiou, S.N. Yannopoulos and T. Ioannides, Biomass-derived graphene-like materials as active electrodes for supercapacitor applications: A critical review, *Chem. Eng. J*., 2022, **446**, 137191.
4. Z. Sun, S. Fang and Y. Hu, 3D graphene materials: From understanding to design and synthesis control, *Chem. Rev*., 2020, **120** (18), 10336–10453.
5. R. Beguin, A. Balducci and E. Frackowiak, Carbons and electrolytes for advanced supercapacitors, *Adv. Mater*., 2014, **26** (14), 2219–2251.
6. K.O. Oyedotun, J. Conradie and K.A. Adegoke, Advances in supercapacitor development: Materials, processes, and applications, *J. Electron. Mater*., 2022, **52** (1), 96–129.
7. J. Zhao and A.F. Burke, Electrochemical capacitors: Materials, technologies and performance, *Energy Stor. Mater*., 2021, **36**, 31–55.
8. A.G. Olabi, Q. Abbas, A. Al Makky and M.A. Abdelkareem, Supercapacitors as next generation energy storage devices: Properties and applications, *Energy*, 2022, **248**, 123617.
9. S. Saini, P. Chand and A. Joshi, Biomass derived carbon for supercapacitor applications: Review, *J. Energy Storage*, 2021, **39**, 102646.
10. D. Zhang, L. Li and Y. Zhang, Metal chalcogenides-based materials for high-performance metal ion capacitors, *J. Alloys Comd*, 2021, **869**, 159352.
11. D.S. Priya, L.J. Kennedy and G.T. Anand, Emerging trends in biomass-derived porous carbon materials for energy storage application: A critical review, *Mater. Today Sustain*., 2023, **21**, 100320.

12. Z. Sun, M. Zheng, H. Hu, H. Dong, B. Lei and Y. Liu, From biomass wastes to vertically aligned graphene nanosheet arrays: A catalyst-free synthetic strategy towards high-quality graphene for electrochemical energy storage, *Chem. Eng. J.*, 2018, **336**, 550–561.
13. X. Luo, S. Chen, T. Hu, Y. Chen and F. Li, Renewable biomass-derived carbons for electrochemical capacitor applications, *SusMat*, 2021, **1** (2), 211–240.
14. L. Sun, C. Tian, M. Li, R. Wang, J. Yin and H. Fu, From coconut shell to porous graphene-like nanosheets for high-power supercapacitors, *J. Mater. Chem. A*, 2013, **1** (21), 6462.
15. J. Xia, N. Zhang, S. Chong, Y. Chen and C. Sun, Three-dimensional porous graphene-like sheets synthesized from biocarbon via low-temperature graphitization for a supercapacitor, *Green Chem.,* 2018, **20** (3), 694-700.
16. L. Guan, L. Pan, Z. Yang, H. Hu and M. Wu, Synthesis of biomass-derived nitrogen-doped porous carbon nanosheests for high-performance supercapacitors, *ACS Sustain. Chem. Eng.*, 2019, **7** (9), 8405–8412.
17. D. Wang, J. Nai, L. Xu and T. Sun, A potassium formate activation strategy for the synthesis of ultrathin graphene-like porous carbon nanosheets for advanced supercapacitor applications, *ACS Sustain. Chem. Eng.*, 2019, **7** (23), 18901–18911.
18. Y. Qi, B. Ge, Y. Zhang, M. Akram and X. Xu, Three-dimensional porous graphene-like biochar derived from Enteromorpha as a persulfate activator for sulfamethoxazole degradation: Role of graphitic N and radicals transformation, *J. Hazard. Mater.*, 2020, **399**, 123039.
19. S. Lu, M. Jin, Y. Zhang, Y. Niu, J. Gao and C. Li, Chemically exfoliating biomass into a graphene-like porous active carbon with rational pore structure, good conductivity, and large surface area for high-performance supercapacitors, *Adv. Energy Mater.*, 2018, **8** (11), 1702545.
20. H. Wang, Z. Xu, J.K. Tak, D. Harfield, A.O. Anyia and D. Mitlin, Interconnected carbon nanosheets derived from hemp for ultrafast supercapacitors with high energy, *ACS Nano*, 2013, **7** (6), 5131–5141.
21. C. Long, X. Chen, L. Jiang, L. Zhi and Z. Fan, Porous layer-stacking carbon derived from in-built template in biomass for high volumetric performance supercapacitors, *Nano Energy*, 2015, **12**, 141–151.
22. B. Liu, M. Yang, D. Yang, H. Li, Graphene-like porous carbon nanosheets for ultra-high rate performance supercapacitors and efficient oxygen reduction electrocatalysts, *J. Power Sources*, 2020, **456**, 227999.
23. Q. Niu, K. Gao, Q. Tang, Y. Zhang, S. Wang and L. Wang, Large-size graphene-like porous carbon nanosheets with controllable N-doped surface derived from sugarcane bagasse pith/chitosan for high performance supercapacitors, *Carbon*, 2017, **123**, 290–298.
24. A. Gopalakrishnan and S. Badhulika, Ultrathin graphene-like 2D porous carbon nanosheets and its excellent capacitance retention for supercapacitor, *J. Ind. Eng. Chem.*, 2018, **68**, 257–266.
25. B. Duan, F. Liu, M. He and L. Zhang, Ag-Fe_3O_4 nanocomposites@chitin microspheres constructed by in situ one-pot synthesis for rapid hydrogenation catalysis, *Green Chem.*, 2014, **16** (5), 2835–2845.
26. W. Tian, Q. Gao, L. Zhang, C. Yang, Z. Li, Y. Tan, W. Qian and H. Zhang, Renewable graphene-like nitrogen-doped carbon nanosheets as supercapacitor electrodes with integrated high energy-power properties, *J. Mater. Chem. A*, 2016, **4** (22), 8690–8699.
27. J. You, M. Li, B. Ding, X. Wu and C. Li, Crab chitin-based 2D soft nanomaterials for fully biobased electric devices, *Adv. Mater.*, 2017, **29** (19), 1606895.
28. B. Wang, S. Li, X. Wu, J. Liu and J. Chen, Biomass chitin-derived honeycomb-like nitrogen-doped carbon/graphene nanosheet networks for applications in efficient oxygen reduction and robust lithium storage, *J. Mater. Chem. A*, 2016, **4** (30), 11789–11799.

29. L. Kong, L. Su, W. Yang, G. Shao and X. Qin, Graphene-like nitrogen-doped porous carbon nanosheets as both cathode and anode for high energy density lithium-ion capacitor, *Electrochim. Acta*, 2020, **349**, 136303.
30. W. Tian, Q. Gao, A. VahidMohammadi, J. Dang, Z. Li, X. Liang, M.M. Hamedi and L. Zhang, Liquid-phase exfoliation of layered biochars into multifunctional heteroatom (Fe, N, S) co-doped graphene-like carbon nanosheets, *Chem. Eng. J.*, 2021, **420**, 127601.
31. D. Yu, X. Zheng, M. Chen and X. Dong, Large-scale synthesis of $Ni(OH)_2$/peach gum derived carbon nanosheet composites with high energy and power density for battery-type supercapacitor, *J. Colloid Interf. Sci.*, 2019, **557**, 608–616.
32. M. Zhang, Z. Song, H. Liu and T. Ma, Biomass-derived highly porous nitrogen-doped graphene orderly supported $NiMn_2O_4$ nanocrystals as efficient electrode materials for asymmetric supercapacitors, *Appl. Surf. Sci.*, 2020, **507**, 145065.
33. D. Li, J. Lin, Y. Lu, Y. Huang, X. He, C. Yu, J. Zhang and C. Tang, MnO_2 nanosheets grown on N-doped agaric-derived three-dimensional porous carbon for asymmetric supercapacitors, *J. Alloys Comd*, 2020, **815**, 152344.
34. B. Liu, Y. Liu, M. Yang and H. Li, MnO_2 nanostructures deposited on graphene-like porous carbon nanosheets for high-rate performance and high-energy density asymmetric supercapacitors, *ACS Sustain. Chem. Eng.*, 2019, **7** (3), 3101–3110.
35. J. Yin, W. Zhang, N.A. Alhebshi, N. Salah and H.N. Alshareef, Synthesis strategies of porous carbon for supercapacitor applications, *Small Methods*, 2020, **4** (3), 1900853.
36. S. Guo, J. Peng, W. Li, K. Yang, L. Zhang, S. Zhang and H. Xia, Effects of CO_2 activation on porous structures of coconut shell-based activated carbons, *Appl. Surf. Sci.*, 2009, **255** (20), 8443–8449.
37. X. Liu, C. He, X. Yu, Y. Bai, L. Ye, B. Wang and L. Zhang, Net-like porous activated carbon materials from shrimp shell by solution-processed carbonization and H_3PO_4 activation for methylene blue adsorption, *Powder Technol.*, 2018, **326**, 181–189.
38. Z. Zhu and Z. Xu, The rational design of biomass-derived carbon materials towards next-generation energy storage: A review, *Renew. Sust. Energy Rev.*, 2020, **134**, 110308.
39. M. Usha Rani, T.N. Rao and A.S. Deshpande, Corn husk derived activated carbon with enhanced electrochemical performance for high-voltage supercapacitors, *J. Power Sources*, 2020, **471**, 228387.
40. X. Fan, C. Yu, J. Yang, M. Zhang and J. Qiu, A layered-nanospace-confinement strategy for the synthesis of two-dimensional porous carbon nanosheets for high-rate performance supercapacitors, *Adv. Energy Mater.*, 2015, **5** (7), 1401761.
41. P. Hao, Z. Zhao, Y. Leng, H. Liu and B. Yang, Graphene-based nitrogen self-doped hierarchical porous carbon aerogels derived from chitosan for high performance supercapacitors, *Nano Energy*, 2015, **15**, 9–23.
42. V. Yang, R.A. Senthil, J. Pan, A. Khan, S. Osman, L. Wang, W. Jiang and Y. Sun, Highly ordered hierarchical porous carbon derived from biomass waste mangosteen peel as superior cathode material for high performance supercapacitor, *J. Electroanal. Chem.*, 2019, **855**, 113616.
43. B. Duan, X. Zheng, Z. Xia, X. Fan, L. Guo, J. Liu, Y. Wang, Q. Ye and L. Zhang, Highly biocompatible nanofibrous microspheres self-assembled from chitin in NaOH/urea aqueous solution as cell carriers, *Angew. Chem. Int. Ed.*, 2015, **54** (17), 5152–5156.
44. O. Pezoti, A.L. Cazetta, O.O. Santos Júnior, J.V. Visentainer and V.C. Almeida, NaOH-activated carbon of high surface area produced from guava seeds as a high-efficiency adsorbent for amoxicillin removal: Kinetic, isotherm and thermodynamic studies, *Chem. Eng. J.*, 2016, **288**, 778–788.
45. Z. Li, D. Guo, Y. Liu, H. Wang and L. Wang, Recent advances and challenges in biomass-derived porous carbon nanomaterials for supercapacitors, *Chem. Eng. J.*, 2020, **397**, 125418.

46. T. Li, R. Ma, X. Xu, S. Sun and J. Lin, Microwave-induced preparation of porous graphene nanosheets derived from biomass for supercapac itors, *Micropor. Mesopor. Mat.*, 2021, **324**, 111277.
47. W. Zhang, R. Cheng, L. Ma and X. He, A review of porous carbons produced by template methods for supercapacitor applications, *New Carbon Mater.*, 2021, **36** (1), 69–81.
48. X. He, N. Zhang, X. Shao, M. Wu, M. Yu and J. Qiu, A layered-template-nanospace-confinement strategy for production of corrugated graphene nanosheets from petroleum pitch for supercapacitors, *Chem. Eng. J.*, 2016, **297**, 121–127.
49. Q. Wang, J. Yan, T. Wei, M. Zhang, X. Jing and Z. Fan, Three-dimensional flower-like and hierarchical porous carbon materials as high-rate performance electrodes for supercapacitors, *Carbon*, 2014, **67**, 119–127.
50. J. Li, Q. Jiang, L. Wei, L. Zhong and X. Wang, Simple and scalable synthesis of hierarchical porous carbon derived from cornstalk without pith for high capacitance and energy density, *J. Mater. Chem. A*, 2020, **8** (3), 1469–1479.
51. X. Xie, X. He, F. Wei, N. Xiao and J. Qiu, Interconnected sheet-like porous carbons from coal tar by a confined soft-template strategy for supercapacitors, *Chem. Eng. J.*, 2018, **350**, 49–56.
52. C. Ban, Z. Xu, D. Wang, Z. Liu and H. Zhang, Porous layered carbon with interconnected pore structure derived from reed membranes for supercapacitors, *ACS Sustain. Chem. Eng.*, 2019, **7** (12), 10742–10750.
53. P. Li, H. Xie, W. Hu, T. Xie, Y. Wang and Y. Zhang, Molten salt and air induced nitrogen-containing graphitic hierarchical porous biocarbon nanosheets derived from kitchen waste hydrolysis residue for energy storage, *J. Power Sources*, 2019, **439**, 227096.